

L-Subshell Coster–Kronig Yields for Tb

Héctor J. Sánchez, Roberto D. Pérez, Marcelo Rubio and Gustavo Castellano

Facultad de Matemática, Astronomía y Física, Universidad Nacional de Córdoba, 5000 Córdoba, Argentina

The synchrotron photoionization method was applied to measure L-subshell Coster–Kronig yields for Tb. This method is based on the capability of tuning the energy of the synchrotron photons producing a selective subshell ionization. A foil sample of Tb was irradiated and characteristic spectra were recorded. Data were analysed using a new formalism (based on a matrix representation) to express x-ray fluorescence intensities involving Coster–Kronig transitions. The results obtained were $f_{12} = 0.201 \pm 0.014$, $f_{13} = 0.281 \pm 0.027$ and $f_{23} = 0.097 \pm 0.016$. These data represent valuable information for spectroscopists, considering the lack of data for L-shell parameters.

INTRODUCTION

Coster–Kronig transitions are atomic processes in which vacancies in multiple shells ‘bubble up’ between subshells. When these transitions are energetically possible, they are the main way by which ionized atoms lose energy. Coster–Kronig processes are the fastest ones that exist in atoms.

Coster–Kronig transitions have theoretical importance because they are very sensitive to the model chosen for representing the atomic structure. Further, they have important experimental applications in x-ray spectrochemical analysis.

Coster–Kronig decay involves electronic transitions between subshells in an atomic shell. They are labelled as f_{ij}^X , denoting the probability that an electron, in the X_j subshell of the X shell, fills in a vacancy of the X_i subshell. Emission processes following a Coster–Kronig transition mainly involve weakly bound electrons. In addition, a very small emission probability of low-energy photons exists.

Theoretical and experimental values of Coster–Kronig yields are scarce and very difficult to obtain. Usually, they present large uncertainties, and discrepancies between theoretical and experimental data are observed.

Traditional methods applied to measuring atomic parameters of L subshells are usually based on coincidence techniques. These methods analyse the coincidence of L emissions with K photons or nuclear radiation. By means of coincidence techniques good results are obtained from some L-subshell coefficients, but these methods cannot be used for determining Coster–Kronig yields associated with the L_1 subshell because the $L_1 \rightarrow K$ transition is forbidden.

Synchrotron radiation (SR) has been used in many x-ray spectrometric experiments and it has helped to develop new experimental techniques in several areas of investigation. In particular, SR has been used to measure L-shell Coster–Kronig transition yields^{1–3} (simply denoted f_{ij}). In addition, Werner and Jitschin⁴ have reported Coster–Kronig yields and ratios of fluorescence yields for L shells in heavy atoms using the

synchrotron photoionization method. This method is based on a selective photoionization of subshells taking advantage of the high degree of tunability of synchrotron radiation.⁵

As an improvement to the coincidence techniques, this method allows one to obtain all Coster–Kronig coefficients and all associated fluorescence yields in multiple shells. Moreover, x-ray fluorescence (XRF) measurements are improved by using synchrotron radiation since higher signal-to-noise ratios can be attained.^{6–8}

In this work, we used the synchrotron photoionization method to obtain the L-shell Coster–Kronig yields for Tb ($Z = 65$).

METHOD

Nowadays, solid-state detectors have sufficient resolution that, together with improved spectrum-fitting programs, it is possible to measure fluorescence intensities from subshells of multiple shells. These intensities, denoted I_i^X , come from some vacancy distribution N_i^X and are related to it through the atomic emission probabilities of the shell X . This relationship is linear and can be expressed as

$$R = \mathcal{A}N \quad (1)$$

where R and N are vectors defined by

$$R_i = I_i^X; \quad N_i = N_i^X \quad (2)$$

The matrix \mathcal{A} can be obtained by means of a careful analysis of the expressions for XRF intensities modified for Coster–Kronig transitions:

$$\mathcal{A} = \mathcal{W} \sum_{i=0}^{n-1} \mathcal{F}^i \quad (3)$$

where n is the number of atomic subshells of X and matrices \mathcal{W} and \mathcal{F} are given by

$$\mathcal{W}_{ij} = \delta_{ij} \omega_{X_i} \Gamma_{X_i} \quad (4)$$

$$\mathcal{F}_{ij} = \begin{cases} 0 & i \leq j \\ \mathcal{F}_{ij}^X & i > j \end{cases} \quad (5)$$

where δ_{ij} is Kronecker's delta, ω_{X_i} is the fluorescence yield of subshell X_i and Γ_{X_i} denotes the emission probability of the characteristic line L_{X_i} .

Noting that for $r \geq n$

$$F^r = 0 \quad (6)$$

it is possible to evaluate Eqn (3):

$$\mathcal{A} = \mathcal{W}(I - \mathcal{F})^{-1} \quad (7)$$

Therefore, \mathcal{A}^{-1} is given by

$$\mathcal{A}^{-1} = (I - \mathcal{F})^{-1} \mathcal{W}^{-1} \quad (8)$$

As we can see, the elements of \mathcal{A}^{-1} have a simple dependence on fluorescence and Coster-Kronig yields. Hence the knowledge of \mathcal{A}^{-1} is equivalent to the knowledge of the atomic emission probabilities.

If n different vacancy distributions N_i^X are created, the matrix \mathcal{A}^{-1} can be obtained from the knowledge of these distributions and the corresponding fluorescence intensities. Now a matrix equation of the form of Eqn (1) can be written:

$$\mathcal{R} = \mathcal{A} \mathcal{N} \quad (9)$$

where now \mathcal{R} and \mathcal{N} are matrices and their columns are given by Eqn (2).

As the n vacancy distributions are all different, matrix \mathcal{R} is invertible and \mathcal{A}^{-1} can be obtained from

$$\mathcal{A}^{-1} = \mathcal{N} \mathcal{R}^{-1} \quad (10)$$

Jitschin and co-workers^{1,4,9} were the first to use the synchrotron photoionization method to generate n different vacancy distributions in the subshells of a multiple shell. This method is based on the possibility of tuning the energy of the photons coming from a synchrotron source. This cannot be achieved using conventional sources such as x-ray tubes and radioactive sources because the flux becomes too low.

If E_{X_n} is the excitation energy of the least bound subshell X_n (see Fig. 1), the first step of our experiment is to excite this subshell with photons of energy E_n , such that

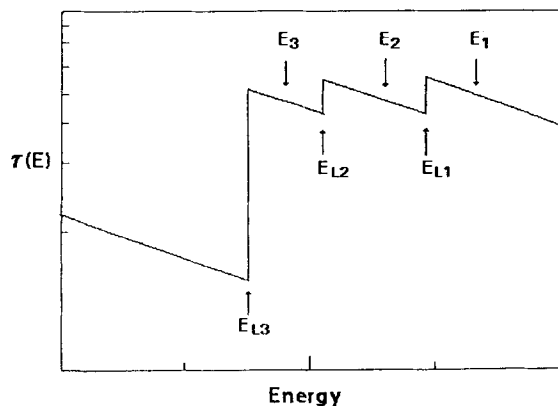


Figure 1. Synchrotron photoionization method applied to the L shell. The absorption edges are excited selectively by photons of energy E_1 , E_2 and E_3 .

$E_{X_n} < E_n < E_{X_{n-1}}$. The fluorescence spectrum emitted by the sample is then recorded.

The following step consists of exciting the absorption edge $E_{X_{n-1}}$ with photons of energy E_{n-1} such that $E_{X_{n-1}} < E_{n-1} < E_{X_{n-2}}$ and recording the emitted fluorescence spectrum. The process is repeated up to the deepest level of the shell.

Theoretical intensities must be calculated in order to relate the n experimental spectra to the coefficients of interest. If we consider a pure sample of thickness d , incident photons of energy E and intensity $I_0(E)$, with incident and take-off angles of 45° , the XRF intensity emitted by the X_i subshell is^{10,11}

$$I_{X_i} = k D_{X_i}(E) M_{X_i}(E) Q_{X_i}(E) I_0(E) \quad (11)$$

with

$$Q_{X_i}(E) = \tau_{X_i}(E) \omega_{X_i} \Gamma_{X_i} \quad (12)$$

$$M_{X_i}(E) = \frac{1 - \exp(-[\mu(E) + \mu(EI_{X_i})] \rho d \sqrt{2})}{\mu(E) + \mu(EI_{X_i})} \quad (13)$$

$$D_{X_i}(E) = \begin{cases} 0 & E < E_{X_i} \\ 1 & E_{X_i} < E \end{cases} \quad (14)$$

where k is an experimental factor depending on the geometry and detector characteristics, EI_{X_i} represents the characteristic emission energy of subshell X_i , $\tau_{X_i}(E)$ is the partial photoelectric absorption coefficient of subshell X_i at energy E , $\mu(E)$ represents the mass attenuation coefficient of the sample to energy E and ρ is the sample density.

In the case of L shell, the above formalism reduces to

$$\mathcal{R} = \begin{pmatrix} \frac{I_{L_1}(E_1)}{M_{L_1}(E_1)} & 0 & 0 \\ \frac{I_{L_2}(E_1)}{M_{L_2}(E_1)} & \frac{I_{L_2}(E_2)}{M_{L_2}(E_2)} & 0 \\ \frac{I_{L_3}(E_1)}{M_{L_3}(E_1)} & \frac{I_{L_3}(E_2)}{M_{L_3}(E_2)} & \frac{I_{L_3}(E_3)}{M_{L_3}(E_3)} \end{pmatrix} \quad (15)$$

$$\mathcal{A} = \begin{pmatrix} \omega_{L_1} \Gamma_{L_1} & 0 & 0 \\ \omega_{L_2} \Gamma_{L_2} f_{12} & \omega_{L_2} \Gamma_{L_2} & 0 \\ \omega_{L_3} \Gamma_{L_3} (f_{13} + f_{12} f_{23}) & \omega_{L_3} \Gamma_{L_3} f_{23} & \omega_{L_3} \Gamma_{L_3} \end{pmatrix} \quad (16)$$

$$\mathcal{N} = k \begin{pmatrix} \tau_{L_1}(E_1) I_0(E_1) & 0 & 0 \\ \tau_{L_2}(E_1) I_0(E_1) & \tau_{L_2}(E_2) I_0(E_2) & 0 \\ \tau_{L_3}(E_1) I_0(E_1) & \tau_{L_3}(E_2) I_0(E_2) & \tau_{L_3}(E_3) I_0(E_3) \end{pmatrix} \quad (17)$$

with

$$\mathcal{W} = \begin{pmatrix} \omega_{L_1} \Gamma_{L_1} & 0 & 0 \\ 0 & \omega_{L_2} \Gamma_{L_2} & 0 \\ 0 & 0 & \omega_{L_3} \Gamma_{L_3} \end{pmatrix} \quad (18)$$

$$\mathcal{F} = \begin{pmatrix} 0 & 0 & 0 \\ f_{12} & 0 & 0 \\ f_{13} & f_{23} & 0 \end{pmatrix} \quad (19)$$

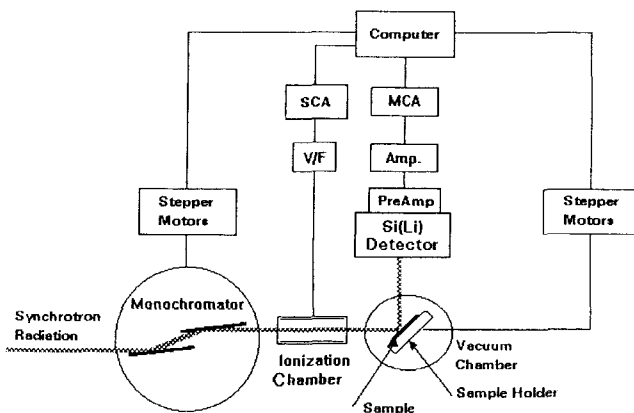


Figure 2. Experimental set-up used in this work.

Finally, L-shell yields are written as

$$\omega_{L_i} = \frac{I_{L_i}(E_i)}{k\tau_{L_i}(E_i)M_{L_i}(E_i)I_0(E_i)\Gamma_{L_i}} \quad \text{for } i = 1, 2, 3 \quad (20)$$

$$f_{23} = \frac{\tau_{L_3}(E_3)M_{L_3}(E_3)I_0(E_3)I_{L_3}(E_2)}{\tau_{L_2}(E_2)M_{L_3}(E_2)I_0(E_2)I_{L_3}(E_3)} - \frac{\tau_{L_3}(E_2)}{\tau_{L_2}(E_2)} \quad (21)$$

$$f_{12} = \frac{\tau_{L_2}(E_2)M_{L_2}(E_2)I_0(E_2)I_{L_2}(E_1)}{\tau_{L_1}(E_1)M_{L_2}(E_1)I_0(E_1)I_{L_2}(E_2)} - \frac{\tau_{L_2}(E_1)}{\tau_{L_1}(E_1)} \quad (22)$$

$$f_{13} = \left\{ \frac{\tau_{L_3}(E_3)I_0(E_3)}{\tau_{L_1}(E_1)I_0(E_1)} \right.$$

$$\times \left[\frac{L_{L_3}(E_3)I_{L_3}(E_1)}{M_{L_3}(E_1)I_{L_3}(E_3)} - \frac{M_{L_2}(E_2)M_{L_3}(E_3)I_{L_2}(E_1)I_{L_3}(E_2)}{M_{L_2}(E_1)M_{L_3}(E_2)I_{L_2}(E_2)I_{L_3}(E_3)} \right] + \frac{\tau_{L_3}(E_2)M_{L_2}(E_2)I_0(E_2)I_{L_2}(E_1)}{\tau_{L_1}(E_1)M_{L_2}(E_1)I_0(E_1)I_{L_2}(E_2)} - \frac{\tau_{L_3}(E_1)}{\tau_{L_1}(E_1)} \quad (23)$$

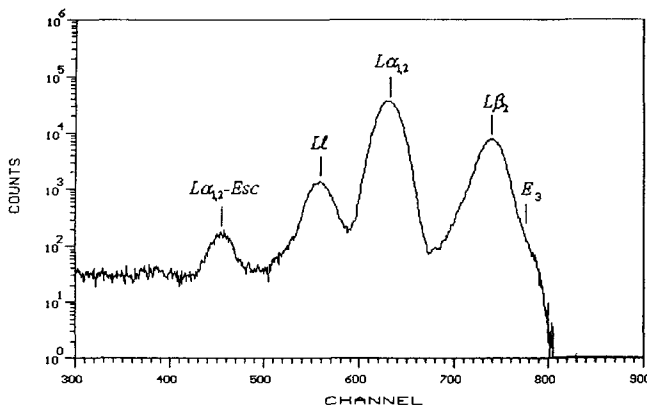


Figure 3. Measured spectrum of Tb excited with photons of 7.7 keV. Only L_3 lines are present.

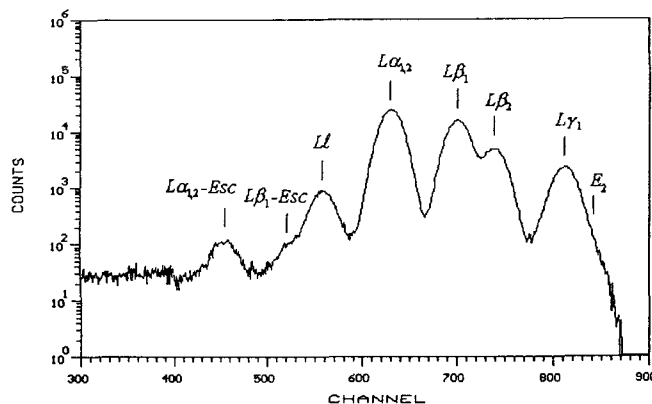


Figure 4. Measured spectrum of Tb excited with photons of 8.4 keV. Only L_3 and L_2 lines are present.

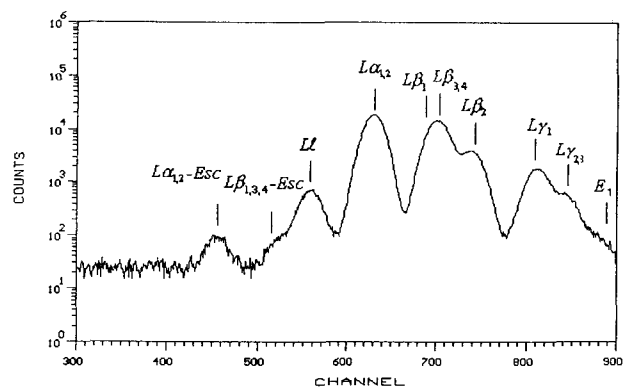


Figure 5. Measured spectrum of Tb excited with photons of 8.9 keV. L_3 , L_2 and L_1 lines are present.

EXPERIMENTAL

The measurements were carried out in the Microanalysis Station of the PWA Group of the Frascati National Laboratories (Italy). The experimental arrangement was described in a previous paper.¹² Figure 2 shows the experimental set-up.

Briefly, conventional XRF or total reflection XRF can be performed in a vacuum chamber. The synchrotron radiation, which comes from a six-pole wiggler, is monochromated by a two-crystal 'channel-cut' monochromator. The incident beam (about 10^{13} photons s^{-1} mrad $^{-1}$ per 0.1% bandwidth for the critical energy) is collimated by two slits at the entrance of the chamber. An ionization chamber with a voltage-to-frequency converter is used for monitoring the beam intensity. The detection system is a typical energy-dispersive set-up. It consists of a Si(Li) solid-state detector, a fast amplifier, an analogue-to-digital converter and a 4K multi-channel buffer. The whole detection system resolution is 170 eV for the $K\alpha$ line for Mn.

The geometry of measurements is 90° and 45° incident and takeoff directions on the plane of the synchrotron electron orbit. This experimental arrangement was set in order to minimize scattered radiation, consequently increasing peak-to-background ratios.¹³

The sample consists of a pure-element foil of Tb ($d = 0.127$ nm). Figures 3–5 show the measured spectra.

DATA ANALYSIS AND RESULTS

Three spectra were obtained by means of the photoionization procedure described under Method. For each

Table 1. L fluorescence yields of Tb

Parameter	This work	Previous work ^a	Theory ^b	Experiment ^c
ω_{L_1}	0.102 ± 0.014	0.090 ± 0.014	0.087	
ω_{L_2}	0.209 ± 0.030	0.194 ± 0.027	0.186	0.165 ± 0.018
ω_{L_3}			0.175	0.188 ± 0.016

^a Ref. 12.^b Puri *et al.*²⁶^c Bambynek *et al.*²⁵

spectrum, the intensity of three lines must be determined. For convenience, we chose the fluorescence lines denoted $L\beta_{3,4}$ (M2, M3 \rightarrow L1), $L\beta_1$ (M4 \rightarrow L2) and $L\alpha_{1,2}$ (M4, M5 \rightarrow L3), since they are the most intense lines of each group.

The resolution of our solid-state detector is not sufficient to separate all the fluorescent lines of the recorded experimental spectra. Thus overlapping effects appear, and fitting procedures are needed. Basically, these procedures fit Gaussian functions to peaks and polynomial functions to the background. In the case of strong overlapping, the intensity of a hidden peak can be predicted using the intensity ratio of this line with respect to a resolved one.

The experimental spectra were analysed with two special programs: AXIL¹⁴ and SPA.¹⁵ Although these programs implement different algorithms to achieve the fitting, the difference between the peak intensities obtained by each program was negligible. The errors of the fitted peak intensities did not exceed 1%.

Calculated intensities were corrected by several factors, the most important of which are described below.

The first correction carried out was related to dead time. Photons arrive randomly at the detector and they have a chance to do this during a period in which the system is not counting. We represent our detection system with a non-paralysable model.¹⁶ The calculations show that this correction is negligible for our solid-state detector.

Detection efficiency was another correction considered. For the solid-state detector, detection efficiency is assumed to be constant in the range of energies used in this work. Therefore, the detected fluorescence intensities are proportional to the emitted ones. This is not true for the ionization chamber, where detection efficiency has a significant dependence on energy.

Escape peaks in the fluorescence spectra were also taken into account. These peaks appear when the characteristic photons of Si escape from the active volume of the detector. Escape peak intensities have to be added to the calculated intensities of the main lines.

Table 2. Coster-Kronig yields of Tb

Parameter	This work	Theory ^a	Experiment ^b
f_{23}	0.097 ± 0.016	0.158	0.066 ± 0.014
f_{12}	0.201 ± 0.014	0.216	0.41 ± 0.36
f_{13}	0.281 ± 0.027	0.334	0.43 ± 0.28

^a Puri *et al.*²⁶^b Bambynek *et al.*²⁵

The last correction considered was related to secondary fluorescence. Enhancement effects are produced because L_1 lines can excite L_2 and L_3 subshells, and L_2 lines can excite the L_3 level. Theoretical calculations of secondary fluorescence were carried out to adjust peak intensities. In most cases the correction was negligible.

Electron correlation effects were neglected in accordance with calculations and considerations of Werner and Jitschin.⁴

Mass attenuation coefficients were taken from McMaster *et al.*¹⁷ and Heinrich,¹⁸ photoelectric cross-sections for L subshells were those reported by Scofield¹⁹ and calculated as in Refs 20 and 21, emission probabilities were obtained from the compilations of Scofield^{22,23} and Khan and Karimi,²⁴ fluorescence yields were taken from Bambynek *et al.*²⁵ and Puri *et al.*²⁶ and the energies of the emission lines were those compiled by Bearden,²⁷ Birks²⁸ and Bearden and Burr.²⁹

In a previous paper,¹² ratios of L fluorescent yields were evaluated for different elements (ratios were necessary to eliminate the influence of the parameter k). In this work, we recalculated these ratios for Tb using the more precise photoelectric cross-section for L subshells reported by Scofield.¹⁹ The choice of these partial cross-sections avoids the use of absorption edge jumps.²⁰ As can be seen in Table 1, the new values are equivalent to the old ones.

On the other hand, Coster-Kronig yields have been shown to be more sensitive to the use of partial cross-sections instead of absorption edge jumps. An important improvement is achieved when Scofield's cross-sections are considered.

Table 2 shows the calculated Coster-Kronig probabilities compared with experimental and theoretical values reported in the literature.^{4,25,26} In general, they agree very well with the other data, showing a better agreement with theoretical values.

Errors were estimated by propagation. Although the experimental factor k [see Eqn (11)] was eliminated from the equations (avoiding the poor statistics of the ionization chamber that monitored the incident beam), the errors were about 10%.

CONCLUSION

Generally, reviews on atomic transition probabilities present mathematical expressions for the relationship between fluorescence intensities and atomic vacancy distributions created in multiple shells. These expressions increase in complexity when more complicated shells are considered. In this work we have developed a simple mathematical formalism based on matrices. Expressions for emission probabilities were obtained in a very simple way within the framework of this formalism.

Finally, the inclusion of Scofield's partial cross-sections instead of the use of absorption edge jumps has proved to give more accurate values of Coster-Kronig yields for Tb.

REFERENCES

1. W. Jitschin, G. Grosse and P. Röhl, *Phys. Rev. A* **39**, 103 (1989).
2. S. L. Sorensen, R. Carr, S. J. Schaphorst, S. B. Whitfield and B. Crasemann, *Phys. Rev. A* **39**, 6241 (1989).
3. S. L. Sorensen, S. J. Schaphorst, S. B. Whitfield and B. Crasemann, *Phys. Rev. A* **44**, 350 (1991).
4. U. Werner and W. Jitschin, *Phys. Rev. A* **38**, 4009 (1988).
5. E. Koch, *Handbook on Synchrotron Radiation*, Vol. 1A. North-Holland, Amsterdam, (1983).
6. A. J. J. Bos, R. D. Vis, H. Verheul, M. Prins, S. T. Davies, D. K. Bowen, J. Makjanić and D. Valković, *Nucl. Instrum. Methods B* **3**, 232 (1984).
7. J. V. Gilfrich, E. F. Skelton, D. J. Nagel, A. W. Webb, S. B. Quadri and J. P. Kirkland, *Adv. X-Ray Anal.* **26**, 313 (1983).
8. A. Iida, Y. Gohshi and T. Matsushita, *Adv. X-Ray Anal.* **28**, 53 (1985).
9. W. Jitschin, G. Materlik, U. Werner and P. Funke, *J. Phys. B* **18**, 1139 (1985).
10. J. Sherman, *Spectrochim. Acta* **7**, 283 (1955).
11. T. Shiraiwa and N. Fujino, *Jpn J. Appl. Phys.* **5**, 886 (1966).
12. H. J. Sánchez, M. Rubio, R. D. Pérez and E. Burattini, *X-Ray Spectrom.* **23**, 267 (1994).
13. A. L. Hanson, *Nucl. Instrum. Methods A* **243**, 583 (1986).
14. P. van Espen, K. Janssens and J. Nobels, *Chemo Lab* **1**, 109 (1986).
15. H. J. Sánchez, *Comput. Phys.* **4**, 407 (1991).
16. G. F. Knoll, *Radiation Detection and Measurements*, p. 120. Wiley, New York (1979).
17. W. H. McMaster, N. Kerr del Grande, J. H. Mallet and J. Hubbell, *Compilation of X-Ray Cross Sections*, Report UCRL 50174, Sect. 2. Lawrence Radiation Laboratory, Livermore, CA (1969).
18. K. Heinrich, in *X-Ray Optics and Microanalysis*, edited by J. Brown and R. Packwood, p. 67. University of Western Ontario, Ontario, Canada (1987).
19. J. H. Scofield, Lawrence Livermore Radiation Laboratory Report No. UCRL-51326. Lawrence Livermore Radiation Laboratory, Livermore, CA (1973) (unpublished).
20. W. Jitschin, U. Werner, G. Materlik and G. D. Doolen, *Phys. Rev. A* **35**, 5038 (1987).
21. R. Stötzel, U. Werner, M. Sarkar and W. Jitschin, *J. Phys. B* **25**, 2295 (1992).
22. J. H. Scofield, *Phys. Rev.* **179**, 9 (1969).
23. J. H. Scofield, *Phys. Rev. A* **9**, 104 (1974).
24. Md. R. Khan and M. Karimi, *X-Ray Spectrom.* **9**, 32 (1980).
25. W. Bambynek, B. Crasemann, R. W. Fink, H. U. Freund and M. Mark, *Rev. Mod. Phys.* **44**, 716 (1961).
26. S. Puri, D. Metha, B. Chand, N. Singh and P. Trehan, *X-Ray Spectrom.* **22**, 358 (1993).
27. J. A. Bearden, *Rev. Mod. Phys.* **39**, 78 (1969).
28. L. S. Birks, in *Handbook of Spectroscopy*, p. 3. CRC Press, Cleveland, OH (1974).
29. J. A. Bearden and A. F. Burr, *Rev. Mod. Phys.* **39**, 125 (1967).